Asian Journal of Chemistry; Vol. 35, No. 6 (2023), 1333-1340

ASIAN JOURNAL OF CHEMISTRY

https://doi.org/10.14233/ajchem.2023.27710

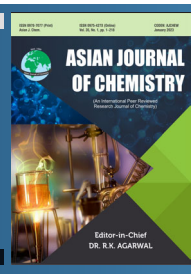

Green Mediated Preparation of Transition Metal Doped Cobalt Oxide Nanoparticles for Wastewater Treatment

A. AJITHA[1,*], K. SEETHALAKSHMI[2], M. MEENA[1] and V. MANIKANDA PRABHU[3]

[1]Department of Physics, S.T. Hindu College (Affiliated to Manonmaniam Sundaranar, Abishekapatti, Tirunelveli) Nagercoil-629002, India
[2]Department of Physics, Sree Devi Kumari Women's College (Affiliated to Manonmaniam Sundaranar, Abishekapatti, Tirunelveli), Kuzithurai-629163, India
[3]Department of Chemical Engineering, Amrita Vishva Vidyapeetham, Coimbatore-641112, India

*Corresponding author: E-mail: ajithavijuav@gmail.com

Received: 20 February 2023; *Accepted*: 8 April 2023; *Published online*: 27 May 2023; AJC-21247

Recent studies have shown that the metal oxide nanoparticles can inhibit bacterial growth on their surfaces due to the creation of super oxide anion when metal ions interact with UV light. One such metal oxide with antibacterial activity against a variety of bacteria is cobalt oxide (Co_3O_4). The optical and anti-pathogen properties of cobalt oxide nanoparticles generated from egg albumin using a microwave-assisted hydrothermal process were studied and optimized by adding copper as a dopant at varying molar concentrations (1, 3 and 5 mol%). Bare and doped samples were analyzed using SEM, energy dispersive X-ray spectroscopy and X-ray diffraction. The resulting structure and small average crystalline size highlight the role of egg albumin in stabilizing and regulating size. A sample with 5 mol% copper doped material exhibited the highest resistance zone to *Escherichia coli* germs. Hence, by controlling the Cu content, both the photocatalytic and antibacterial properties can be enchanced.

Keywords: Nanoparticles, Egg albumin, Antibacterial activity, Photocatalytic deterioration.

INTRODUCTION

One of the most important environmental problems currently the whole world facing is the water contamination. Water that has been contaminated by sewage and industrial effluents is also a result of pathogens [1,2]. Many illnesses that can be fatal to living things are mostly caused by bacterial infections. So, it is imperative to enter a safe, non-toxic and healthy environment in order to produce nanoparticles in a green manner [3]. With less toxic chemical synthesis, clean solvents, energy-efficient design and the utilization of renewable raw materials, green synthesis of nanoparticles advances green chemistry ideas [4]. Nanoparticles are essential to the process of purifying waste water. Due to its use in photocatalysis and antibacterial applications, metal oxide nanoparticles have attracted attention [5]. Because of their high surface area and unique combination of structural, optical and catalytic activities, Co_3O_4 nanoparticles are an attractive candidate for use in the biomedical applications [6].

Elemental doping has recently emerged as a practical and effective technique for capturing the optical and electrical abundance of cobalt oxide nanoparticles [7]. The combination of intrinsic and extrinsic Cu doping would therefore be very stimulating in catalytic and antibacterial applications and it is anticipated to bring about a considerable improvement in performance compared to pristine Co_3O_4. The protein egg albumin is renowned for its ability to gel and mixture. Egg white can be used as a binder, cum gel and moulding material because it is soluble in water and can combine with metal ions [8]. It is also affordable, readily available and environmentally beneficial. Although there have been conflicting reports regarding the manufacturing of egg albumin nanomaterials, it has been reported that the proteins can interact with metal and metal oxide nanoparticles and promote nucleation [9,10]. Egg albumin can therefore be utilized to prepare nanomaterials with some uniformity in their shape. An effective way to create inorganic materials with a smaller size and consistency than those nucleated by traditional heating is using microwave-assisted hydrothermal

processing [11,12]. The aim of the current study is to prepare cobalt oxide nanoparticles using copper as dopant in a range of concentrations using a hydrothermal approach with egg albumin acting as an emulsifier and regulator. The antibacterial and photocatalytic properties of the green-mediated doped cobalt oxide utilizing egg albumin were also evaluated for the first time.

EXPERIMENTAL

A Shimadzu X-ray diffractometer that is monochromated with Cu*K*α radiation in the 2θ range of 10º to 80º at a 10 º/min scan rate was used to acquire the PXRD patterns for calcined samples. The Jasco V-750 spectrometer was used to capture the UV-Vis Diffusion spectra between 200 and 800 nm. The structural morphology was studied using GEM-300, Carl Zeiss, Germany, whereas the Oxford Instruments X-Max was used for the energy dispersive X-ray spectroscopy of the elements. The Agar disk diffusion method was used to test the antibacterial activity of the nanoparticles. The photocatalytic degradation of the methylene blue dye was investigated under the influence of visible light in both the absence and presence of a catalyst. The treated samples from the predefined time range were subjected to UV spectral analysis between 200 and 800 nm in order to analyze the kinetic studies.

Synthesis: A microwave aided hydrothermal procedure employing egg albumin was used to make both pure and copper-doped Co_3O_4 nanoparticles. Cobalt acetate and egg albumin were employed in the current investigation as precursors to create pure and Cu doped cobalt oxide nanoparticles. Separately, the precursors in a 1:3 ratio were taken and dissolved in distilled water. Cobalt acetate solution was continuously stirred followed by the addition of freshly made egg albumin solution dropwise. The final product was then heated for roughly 30 min in a home microwave oven. Egg albumin breaks down under microwave radiation to produce oxygen ions and serves as a binder and moulding substance. Colloidal precipitate was obtained as the solvent totally evaporated. This colloidal precipitate was rinsed with doubly distilled water many times before being dried. The organic impurities in the dried sample were removed using acetone wash. The powder samples were then calcined at 700 ºC for 1 h. The same steps were taken for the preparation of other samples when copper was doped at levels of 1, 3 and 5 mol%.

RESULTS AND DISCUSSION

P-XRD studies: Fig. 1 shows the PXRD patterns of Cu-doped and undoped Co_3O_4 samples. In the standard spectrum of face-centered cubic crystalline Co_3O_4 as per JCPDS card no. (# 43-1003), the diffractogram of pristine Co_3O_4 nanoparticles closely matches the diffraction peak at 2θ values of 19.03º, 31.21º, 36.90º, 38.55º, 44.90º, 55.00º, 59.35º, 65.40º, 68.76º, 69.78º, 77.90º and 78.38º which corresponds to (1 1 1), (2 2 0), (3 1 1), (2 2 2), (4 4 0), (5 3 1), (4 4 2), (5 3 3), (6 2 2) crystal planes, respectively. A lower angle peak shift in the diffraction pattern is caused by copper inclusion. With the rise in Cu concentrations, no additional peaks connected to the impurity phase were discovered, proving that the phases are stable and that Cu ions are uniformly incorporated into the Co_3O_4 lattice. The intensity and crystallinity both decrease with increasing copper concentration, possibly as a result of the strain formed in the Co_3O_4 lattice due to the incorporation of Cu ions, which is well in line with the findings reported by several researchers [13-15].

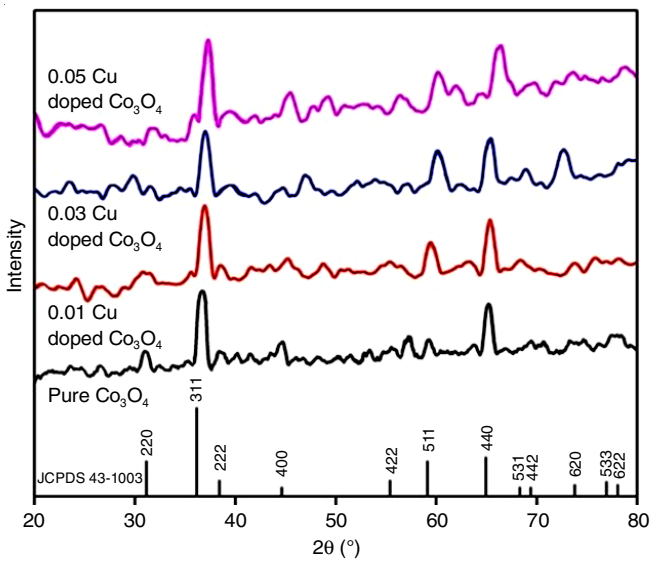

Fig. 1. Powder-X-ray diffractogram of pure Co_3O_4 and Cu doped Co_3O_4

The Debye-Scherrer's formula [16] was used to determine the average crystallite size of the prepared samples. Using unit cell Win software, the lattice parameters were calculated. All calculated values, along with the obtained average crystallite size, were listed in Table-1. The unit cell volume of Cu-doped Co_3O_4 decreased at higher concentrations, indicating a quantitative substitution of Cu ions in the lattice site. Dislocation density, which is correlated with the density of defects in the sample, is defined as the dimension of a dislocation per unit volume. As dopant concentrations are increased, dislocation densities become aberrant. Table-1 shows that the dislocation rises with increasing Cu doping concentration indicating that

TABLE-1
UNIT CELL PARAMETERS CALCULATED FROM XRD PATTERN AND PARTICLE SIZE FROM SEM HISTOGRAM

Sample	Pristine	1 mol % Cu	3 mol % Cu	5 mol % Cu
Lattice parameter, a (Å) (± 0.01)	8.10	8.09	8.08	8.07
Volume, V (Å^3) (± 1.8)	531.2	529.7	528.4	526.9
Average crystallite size, D (nm) (± 0.03)	20.45	16.74	15.63	13.04
Average strain × 10^{-3} (± 0.5)	1.55	1.87	2. 23	2.71
Dislocation density × 10^{-12} (± 1.3)	3.20	3.67	4.1	6.26
Particle size, D (nm) from SEM histogram	24	21	16	15

Cu caused defects in the Co_3O_4 matrix, which decreased crystallinity as a result of stress generation and lattice contraction [17].

SEM studies: The SEM images of bare and doped with copper samples are shown in Fig. 2. The morphology and grain size of all calcined Co_3O_4 nanoparticles were assessed using SEM micrographs at high magnification. The greatly enlarged micrograph reveals that the tiny particles banded together to form a structure like a bunch. The bunch-like structure changed as the Cu content was raised, resulting in the creation of denser formations. Clusters appear, indicating that when concentrations rise, the strain does as well.

Particle size distribution: Fig. 3 shows that as copper dopant concentration increases, the particle size of the grown nanoparticles decreases.

EDX studies: The elemental composition determined by EDX strictly indicates the presence of cobalt and oxygen peaks alone for pure Co_3O_4, whereas Cu peaks are also present in Cu doped Co_3O_4, indicating the purity of the samples. The images (Fig. 4) showed that the particles are uniformly coated with oxides. The presence of cobalt is represented by peaks near 0.8 and 7 KeV. The peak near 0.5 KeV reflects the oxygen element and the peaks near 0.1, 8 and 9 KeV comprise the copper element.

UV-DRS studies: The UV-Vis DRS spectra of pure and Cu-doped cobalt oxide nanoparticles were obtained in the 200-800 nm range. Fig. 5 shows the recorded reflectance of proposed samples, which shows two reflectance bands at 223 and 870 nm. The metal charge transfer process is assigned by the double band. The optical properties of Co_3O_4 are affected by a number of variables, including surface roughness, porosity and photogenerated electron-hole carriers. The red shift phenomena may be linked to the quantum effect because the absorption edge shifts towards the longer wavelength side (222 nm to 224 nm) [18]. A quantum confinement effect involving small nanoparticles is supported by the reduction in the band gaps of the synthesized Co_3O_4 nanoparticles (Table-2).

TABLE-2
BANDGAP ENERGY OF Co_3O_4 AND Cu DOPED Co_3O_4

Sample	E_g (eV)
Pristine	1.30 and 4.11
Cu 0.01	1.26 and 4.01
Cu 0.03	1.16 and 3.91
Cu 0.05	1.08 and 3.61

Fig. 6 shows the plots of hν *vs*. $[(F(R)h\nu]^2$ for Cu-doped Co_3O_4. The Co_3O_4 that has been doped with Cu exhibits a shift

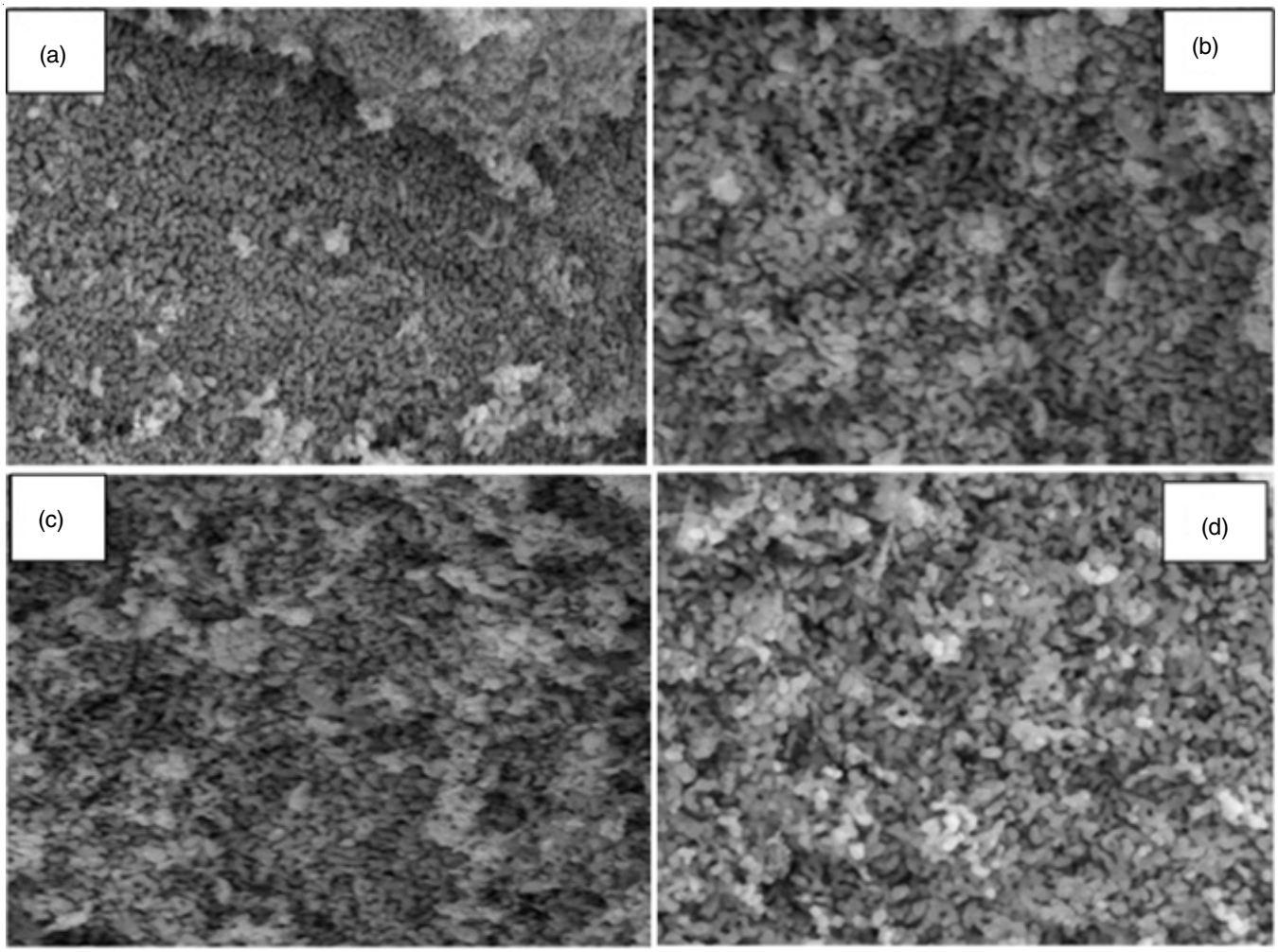

Fig. 2. SEM images of pure Co_3O_4 and Cu doped Co_3O_4

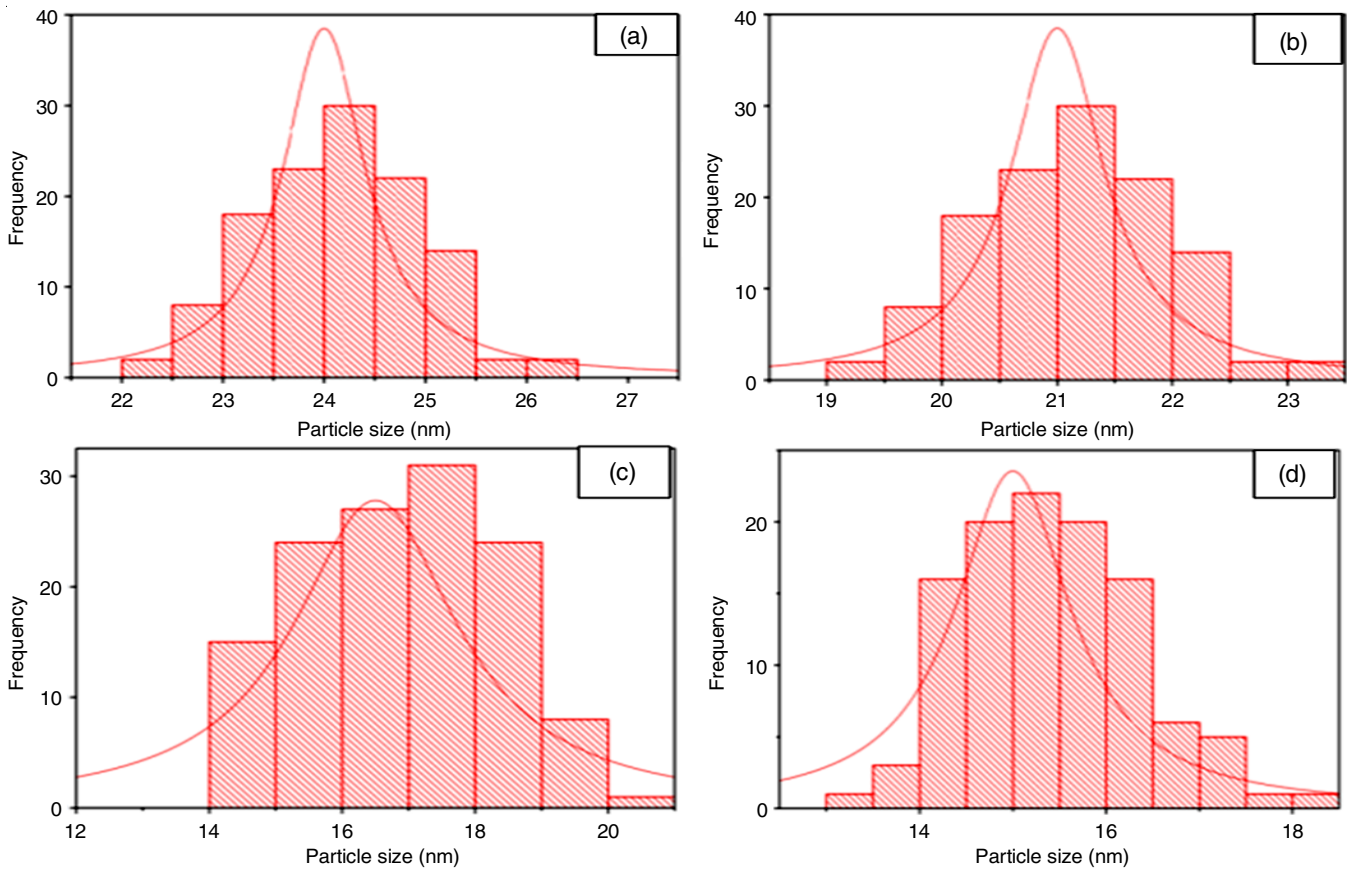

Fig. 3. Particle size histogram of pure Co_3O_4 and Cu doped Co_3O_4

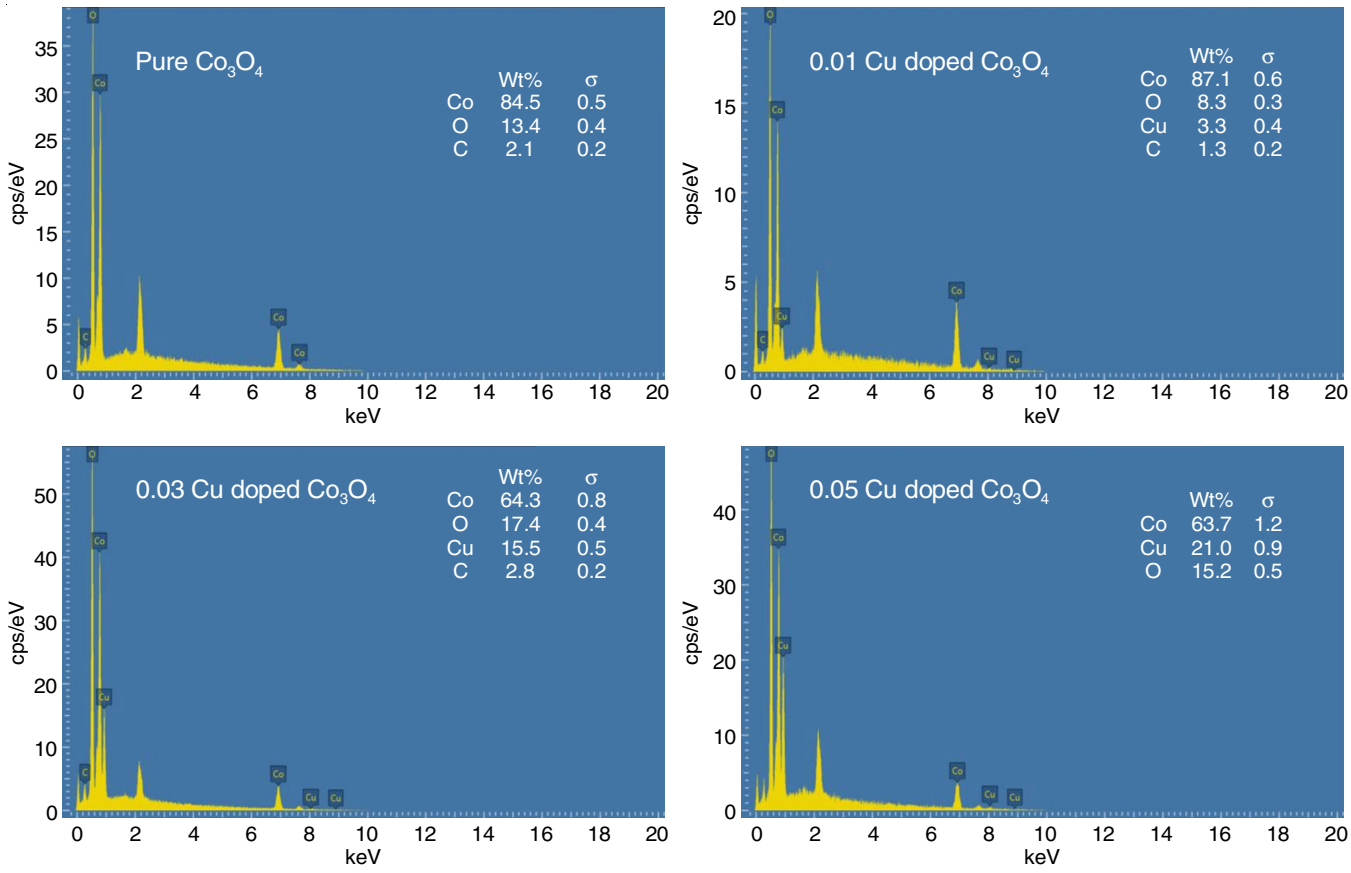

Fig. 4. EDX spectra of pure Co_3O_4 and Cu doped Co_3O_4

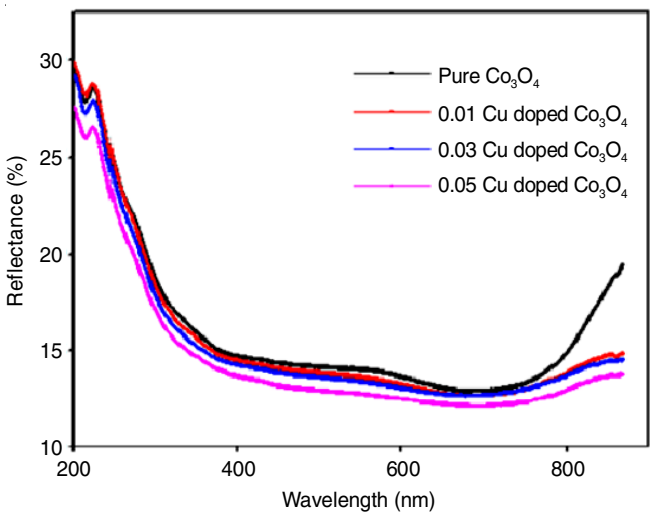

Fig. 5. UV spectrum of pure Co_3O_4 and Cu doped Co_3O_4

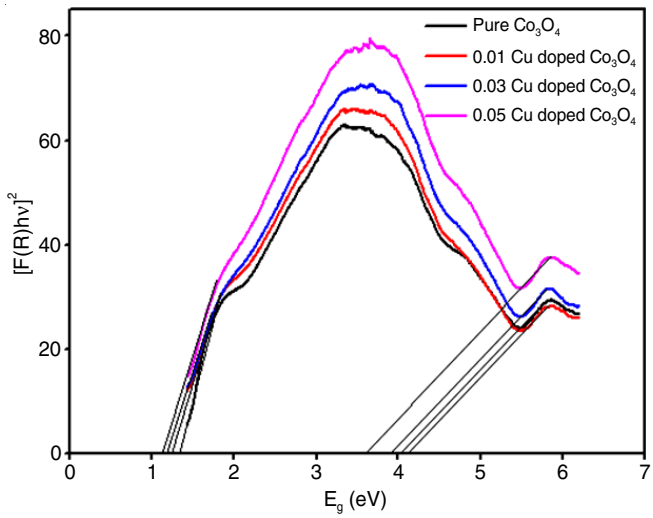

Fig. 6. Tauc plot of pure Co_3O_4 and Cu doped Co_3O_4

in bandgap proportional to the concentration of copper present. It has been suggested that the cation may be replaced by an electron from a new state in the gap through spin-exchange interactions between the band electrons and the electrons of the transition metal ion [18].

When the concentration of Cu increases, the direct band gap energy decreases. The development of more energy levels in doped Co_3O_4 than in pristine Co_3O_4 as a result of the interstitial of Cu ions into the cobalt lattice may be the cause of the reduced band gap energy. The appropriate applications of photocatalytic deterioration are attributed by the nanoparticles' decreasing band gap energy [19]. It has also been stated that optoelectronic devices are made with a band gap of 1 to 2 eV [20].

Antibacterial activity: The main idea behind this method is to predict antibiotic resistance by monitoring the expansion of inhibition zone (ZOI) around the powered sample in order to test the antibacterial activity of the calcined samples against *E. coli* using the aminoglycoside antibiotic drug amikacin as control. The inhibitory effect of pure and Cu-doped Co_3O_4 on Gram-negative *Escherichia coli* bacteria is shown in Fig. 7.

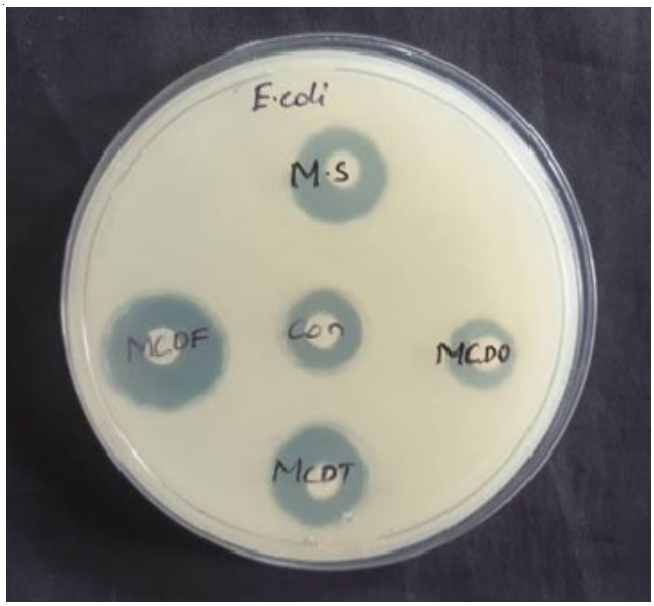

Fig. 7. Inhibitory action of pure Co_3O_4 and Cu doped Co_3O_4.

The diameter of the inhibition zone increases as Cu dopant concentration increases (Table-3). Thus, the prepared Cu doped cobalt oxide nanoparticles are found to have good antibacterial activity with a greater zone of inhibition and an average crystallite size of 20 nm [21]. The obtained ZOI is more than the previously reported biosynthesis values [22,23]. Egg albumin is therefore more effective than plant mediated nanoparticles at enhancing the antibacterial activity. Small particles can easily penetrate the bacterial cell wall, causing DNA to be broken, the release of proteins, minerals and genetic material and finally cell death [24].

TABLE-3
ANTIBACTERIAL ACTIVITY ON
PURE Co_3O_4 AND Cu DOPED Co_3O_4

Sample	Control amikacin	Pristine	0.01 mol	0.03 mol	0.05 mol
ZOI (mm)	14	15	17	18	21

Photocatalytic activity: Fig. 8 shows the photocatalytic activity of undoped Co_3O_4 and Co_3O_4 doped with Cu showed methylene blue decoloration with increasing irradiation duration. At 290 and 663 nm, respectively, the weaker and stronger absorption bands of the methylene blue dye were observed. The distance between the two absorption maxima decreased over time. A rapid degradation of the chromophores responsible for the dyes' colours is reflected in the diminishing peak intensity. It was demonstrated that methylene blue dye with 5 mol% Cu-doped nanoparticles degrades more rapidly than the pure sample. This could be as a result of defects brought on by a high Cu content and shrinking particle size [25]. Yet, the percentage of dye deterioration increases as Cu dopant levels grow and time passes swiftly.

Electronic structure, catalyst concentration, dye pH, light source, particle size, surface morphology and optical transitions of a material are some of the elements that affect dye deterioration. The catalytic activity is greatly influenced by the energy

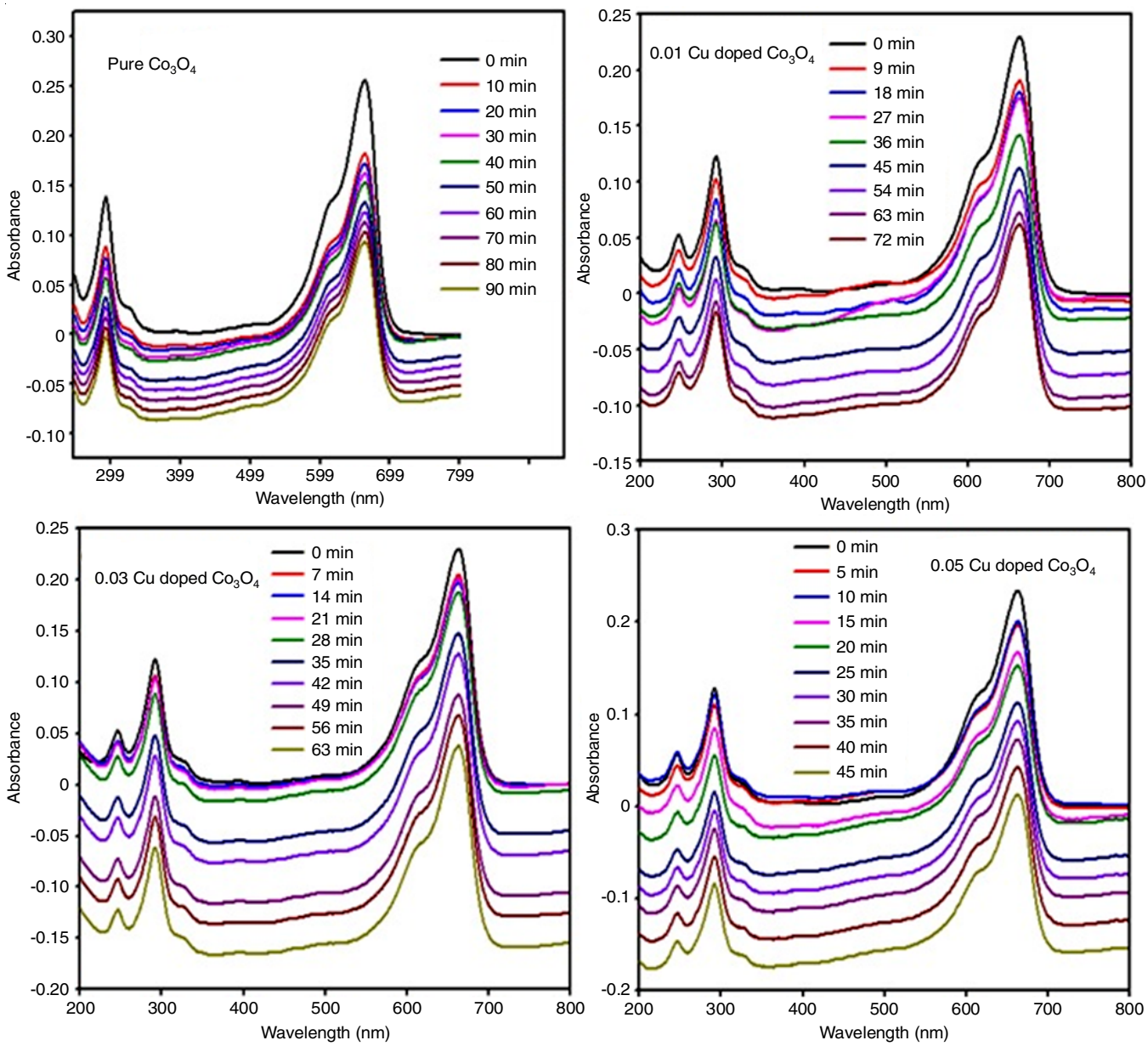

Fig. 8. Photocatalytic deterioration of methylene blue dye using pure Co_3O_4 and Cu doped Co_3O_4

levels present in a metal oxide semiconductor and by tailoring the bandgap to the required level. Such standards are also established by the current examination of the prepared nanoparticles.

These criteria of generated nanoparticles optimized for obtaining the highest degradation efficiency. Deterioration efficiency is calculated by the following formula [26]:

$$\eta\ (\%) = \left(A_0 - \frac{A}{A_0} \right) \times 100$$

where η is the deterioration efficiency, A_0 is the initial absorbance at zero interval of time, A is the absorbance after irradiation of light at various time intervals.

Fig. 8 shows UV-Vis absorption spectra of methylene blue after photo-irradiation with Co_3O_4 and 0.01, 0.03 and 0.05 mol% Cu doped Co_3O_4 indicate that the latter decolourizes methylene blue more quickly than pure Co_3O_4 and the other two mole concentrations. The rate of decolorization was determined by observing the changes in the intensity of methylene blue absorption, which peaks around 663 nm. Co_3O_4 was found to degrade methylene blue at a rate of about 64% in 90 min, but Co_3O_4 that had been doped with 0.01, 0.03 and 0.05 mol% Cu did so at rates of about 72%, 83% and 94% in 72, 63 and 45 min, respectively (Fig. 9). With low consumption and excellent degrading efficiency, 5 mol% Cu-doped cobalt oxide is a possible photocatalyst that offers the best solution for resolving water pollution issues.

Conclusion

Nanoparticles of pure and copper-doped Co_3O_4 were successfully synthesized using a simple microwave-assisted hydrothermal process including egg albumin. Egg albumin is a superb bio-oxygen precursor for producing metal oxide nanoparticles *via* a green process, as shown by the observed shape

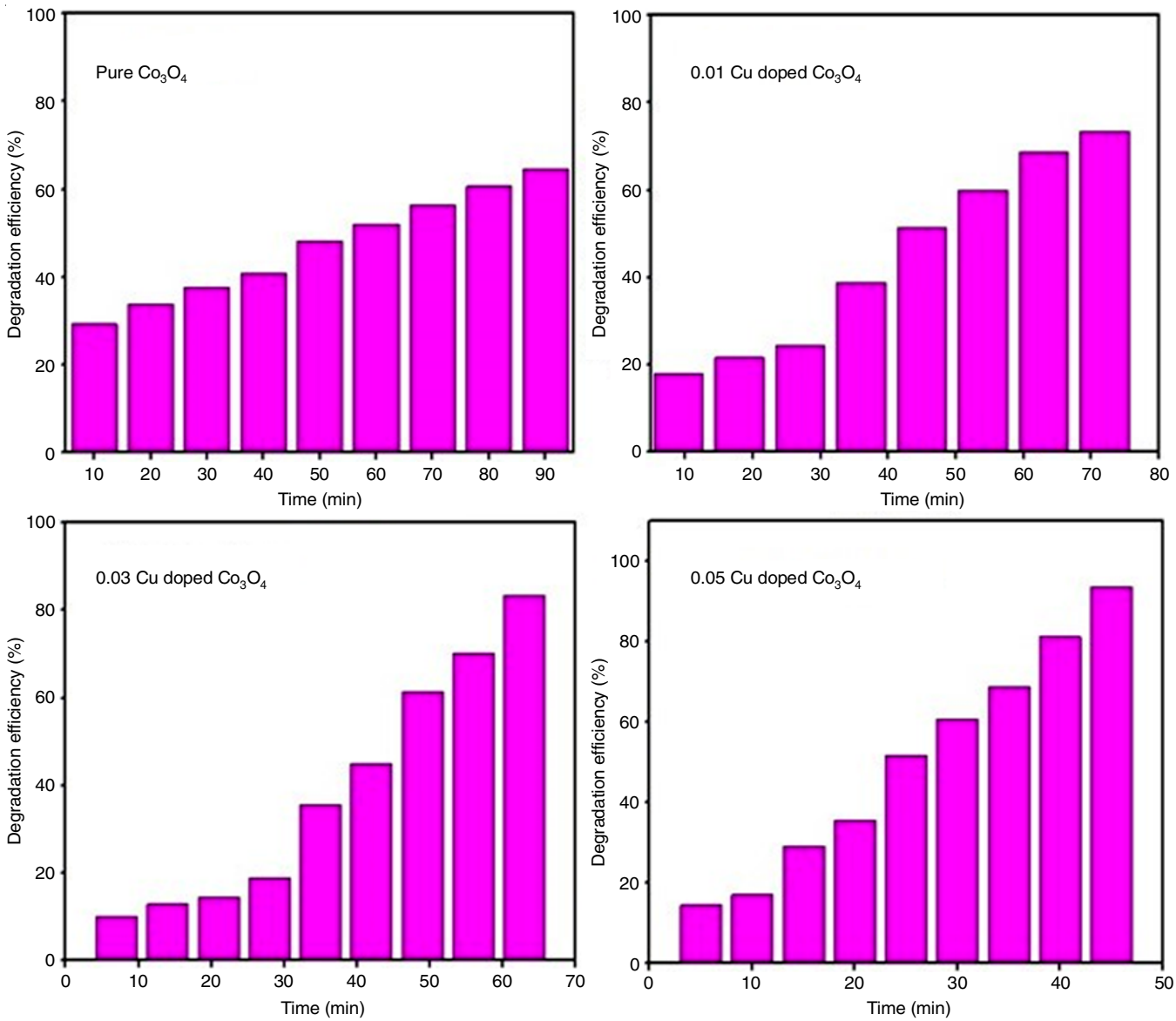

Fig. 9. Photocatalytic deterioration percentage of methylene blue dye using pure Co_3O_4 and Cu doped Co_3O_4

and crystalline size using XRD and SEM techniques. The use of egg albumin also reduces the toxicity of generated particles and their tendency to agglomerate. About 94% of methylene blue dye was degraded in shorter time and with less catalyst, demonstrating the possibility of modifying the photocatalytic behaviour of Co_3O_4 nanoparticles to treat textile industry wastewater.

CONFLICT OF INTEREST

The authors declare that there is no conflict of interests regarding the publication of this article.

REFERENCES

1. S. Some, R. Mondal, D. Mitra, D. Jain, D. Verma and S. Das, *Energy Nexus*, **1**, 100008 (2021); https://doi.org/10.1016/j.nexus.2021.100008
2. M. Ismail, K. Akhtar, M.I. Khan, T. Kamal, M.A. Khan, A. M. Asiri, J. Seo and S.B. Khan, *Curr. Pharm. Des.*, **25**, 3645 (2019); https://doi.org/10.2174/1381612825666191021142026
3. B. Bhardwaj, P. Singh, A. Kumar, S. Kumar and V. Budhwar, *Adv. Pharm. Bull.*, **10**, 566 (2020); https://doi.org/10.34172/apb.2020.067
4. M.A.E. Aleem Ali El-Remaily, A.M. Abu-Dief and R.M. El-Khatib, *Appl. Organomet. Chem.*, **30**, 1022 (2016); https://doi.org/10.1002/aoc.3536
5. S. Vasantharaj, S. Sathiyavimal, P. Senthilkumar, F. LewisOscar and A. Pugazhendhi, *J. Photochem. Photobiol. B*, **192**, 74 (2019); https://doi.org/10.1016/j.jphotobiol.2018.12.025
6. D. Letsholathebe, F.T. Thema, K. Mphale, H.E.A. Mohamed, K.J. Holonga, R. Ketlhwaafetse and S. Chimidza, *Mater. Today: Proceed.*, **36**, 499 (2020); https://doi.org/10.1016/j.matpr.2020.05.205
7. K. Qi, X. Xing, A. Zada, M. Li, Q. Wang, S.-Y. Liu, H. Lin and G. Wang, *Ceramics Int.*, **46**, 1494 (2019); https://doi.org/10.1016/j.ceramint.2019.09.116
8. S. Dhara and P. Bhargava, *J. Am. Ceram. Soc.*, **86**, 1645 (2003); https://doi.org/10.1111/j.1151-2916.2003.tb03534.x
9. M.J. Limo, A. Sola-Rabada, E. Boix, V. Thota, Z.C. Westcott, V. Puddu and C.C. Perry, *Chem. Rev.*, **118**, 11118 (2018); https://doi.org/10.1021/acs.chemrev.7b00660
10. S.S. Teske and C.S. Detweiler, *Int. J. Environ. Res. Public Health*, **12**, 1112 (2015); https://doi.org/10.3390/ijerph120201112

11. A.A. Rempel, E.A. Kozlova, T.I. Gorbunova, S.V. Cherepanova, E.Y. Gerasimov, N.S. Kozhevnikova, A.A. Valeeva, E.Y. Korovin, V.V. Kaichev and Y.A. Shchipunov, *Catal. Commun.*, **68**, 61 (2015); https://doi.org/10.1016/j.catcom.2015.04.034
12. L. Ling, L. Liu, Y. Feng, J. Zhu and Z. Bian, *Chin. J. Catal.*, **39**, 639 (2018); https://doi.org/10.1016/S1872-2067(17)62980-2
13. S. Faniband, C.C. Vidyasagar, V.M. Jiménez-Pérez, V.M. Jiménez-Pérez, Mounesh and A.H. Shridhar, *React. Chem. Eng.*, **7**, 1847 (2022); https://doi.org/10.1039/D2RE00117A
14. M. Zahan and J. Podder, *Biointerface Res. Appl. Chem.*, **12**, 6321 (2022); https://doi.org/10.33263/BRIAC125.63216335
15. 13 Z. Sheikhi Mehrabadi, A. Ahmadpour, N. Shahtahmasebi and M.M. Bagheri Mohagheghi, *Phys. Scr.*, **84**, 015801 (2011); https://doi.org/10.1088/0031-8949/84/01/015801
16. N. Senthilkumar, E. Vivek, M. Shankar, M. Meena, M. Vimalan and I.V. Potheher, *J. Mater. Sci. Mater. Electron.*, **29**, 2927 (2018); https://doi.org/10.1007/s10854-017-8223-5
17. I.S. Okeke, K.K. Agwu, A.A. Ubachukwu, I.G. Madiba, M. Maaza, G.M. Whyte and F.I. Ezema, *Vacuum*, **187**, 110110 (2021); https://doi.org/10.1016/j.vacuum.2021.110110
18. C. Wang, H. Shi and Y. Li, *Appl. Surf. Sci.*, **257**, 6873 (2011); https://doi.org/10.1016/j.apsusc.2011.03.021
19. M.M. Khan, S.A. Ansari, D. Pradhan, M.O. Ansari, D.H. Han, J. Lee and M.H. Cho, *J. Mater. Chem. A Mater. Energy Sustain.*, **2**, 637 (2014); https://doi.org/10.1039/C3TA14052K
20. A. Kumar and P.K. Ahluwalia, *Eur. Phys. J. B*, **85**, 186 (2012); https://doi.org/10.1140/epjb/e2012-30070-x
21. A.K. Singh, *Curr. Res. Green Sustain. Chem.*, **5**, 100270 (2022); https://doi.org/10.1016/j.crgsc.2022.100270
22. M. Hafeez, R. Shaheen, B. Akram, Zain-ul-Abdin, S. Haq, S. Mahsud, S. Ali and R.T. Khan, *Mater. Res. Express*, **7**, 025019 (2020); https://doi.org/10.1088/2053-1591/ab70dd
23. R. Govindasamy, V. Raja, S. Singh, M. Govindarasu, S. Sabura, K. Rekha, V.D. Rajeswari, S.S. Alharthi, M. Vaiyapuri, R. Sudarmani, S. Jesurani, B. Venkidasamy and M. Thiruvengadam, *Molecules*, **27**, 5646 (2022); https://doi.org/10.3390/molecules27175646
24. K. Ravichandran, P. Sathish, S. Snega, K. Karthika, P.V. Rajkumar, K. Subha and B. Sakthivel, *Powder Technol.*, **274**, 250 (2015); https://doi.org/10.1016/j.powtec.2014.12.053
25. T. Warang, N. Patel, R. Fernandes, N. Bazzanella and A. Miotello, *Appl. Catal. B*, **132-133**, 204 (2013); https://doi.org/10.1016/j.apcatb.2012.11.040
26. S. Alkaykh, A. Mbarek and E.E. Ali-Shattle, *Heliyon*, **6**, e03663 (2020); https://doi.org/10.1016/j.heliyon.2020.e03663